REPORT DOCUMENTATION PAGE

Form Approved
OMB No. 0704-0188

1. AGENCY USE ONLY (Leave blank)	2. REPORT DATE	3. REPORT TYPE AND DATES COVERED
	12/31/97	Final Report 960901-970831

4. TITLE AND SUBTITLE

A Direct Comparison of Passive Polarimetry and Scatterometry Under Low- and High-Wind Condtions

5. FUNDING NUMBERS

N00014-96-1-0698

6. AUTHOR(S)

Calvin T. Swift
James R. Carswell

7. PERFORMING ORGANIZATION NAME(S) AND ADDRESS(ES)

University of Massachusetts
Electrical and Computer Engineering Department
Microwave Remote Sensing Laboratory
Amherst, MA 01003

8. PERFORMING ORGANIZATION REPORT NUMBER

9. SPONSORING/MONITORING AGENCY NAME(S) AND ADDRESS(ES)

Office of Naval Research Regional Office Boston
495 Summer Street, Room 103
Boston, MA 02210-2109

10. SPONSORING/MONITORING AGENCY REPORT NUMBER

11. SUPPLEMENTARY NOTES

12a. DISTRIBUTION/AVAILABILITY STATEMENT

Approved for public release; distribution unlimited

13. ABSTRACT *(Maximum 200 words)*

The University of Massachusetts Microwave Remote Sensing Laboratory (MIRSL) gathered coincident active and passive measurements of the ocean surface from the NASA Wallops P3 during the Ocean Wind Imaging (OWI) Experiment. The experiment consisted of five missions flown over the Labrador Sea. Surface winds from 8 to 16 $m \cdot s^{-1}$ were sampled, and approximately thirty hours of data were collected. The passive measurements were obtained with a novel Ka-band conically scanning passive polarmeter (KASPR) that simultaneously measures the four brightness temperature Stokes parameters by using a correlation receiver. The active measurements were collected by a conically scanning C-band scatterometer (CSCAT) that simultaneously measures the backscatter at four separate incidence angles. Analysis of the passive data shows a wind directional signature in the vertically and horizontally polarized brightness temperature measurements at the high winds. For vertical polarization, the wind direction signature is best described by a two-term Fourier cosine series, while for horizontal polarization, the wind direction signature is described by a three-term Fourier cosine series. This report presents these results as well as summarizes the data obtained and the future analysis plans.

14. SUBJECT TERMS

15. NUMBER OF PAGES 15

16. PRICE CODE

17. SECURITY CLASSIFICATION OF REPORT	18. SECURITY CLASSIFICATION OF THIS PAGE	19. SECURITY CLASSIFICATION OF ABSTRACT	20. LIMITATION OF ABSTRACT

FINAL REPORT

A Direct Comparison of Passive Polarimetry and Scatterometry Under Low and High Wind Conditions

Submitted by:

Microwave Remote Sensing Laboratory
University of Massachusetts
Amherst, MA 01002

December 31, 1997

N00014-96-1-0698

This report summarizes the work performed by the Microwave Remote Sensing Laboratory (MIRSL) at the University of Massachusetts (UMASS) for the ONR grant entitled, "A Direct Comparison of Passive Polarimetry and Scatterometry Under Low and High Wind Conditions".

Goals

The following were the proposed objectives:

- Collect coincident scattering and emission measurements of the ocean surface at intermediate incidence angles from an aircraft platform.
- Evaluate passive polarimetry for ocean wind vector retrieval.
- Compare passive polarimetric and backscatter measurements of the ocean surface under high wind conditions.

Introduction

To meet the goals specified above, MIRSL proposed to install its C-band scatterometer (CSCAT) and Ka-band scanning polarimetric radiometer (KASPR) on the NASA Wallops P3 and collect active and passive ocean measurements with these instruments during the Ocean Winds Imaging (OWI) Experiment. MIRSL modified KASPR by adding a scan mirror so that its beam could be conically scanned at 47.5° incidence at rates as high as 30 rpm.

The OWI Experiment was a success. Five missions were flown over the Labrador Sea and winds from approximately 8 to 16 $m \cdot s^{-1}$ were sampled. Despite the harsh environment, the instruments operated almost continuously with the exception of the transit flight back to base on the first mission. The next three sections will describe the OWI Experiment, the data obtained, and the analysis that has been performed so far.

OWI Experiment

In January, 1997 a unique complement of passive and active instruments were integrated onto the NASA Wallops P3 to gather scattering and emission measurements of the ocean surface. The instruments included the UMASS CSCAT and KASPR, the four band tri-polarimetric scanning radiometer (PSR), the nadir-viewing Ka-band polarimetric radiometer (KAPOL) and the NASA Ku-band Radar Ocean Wave Spectrometer (ROWS). Figure 1 shows the installation layout.

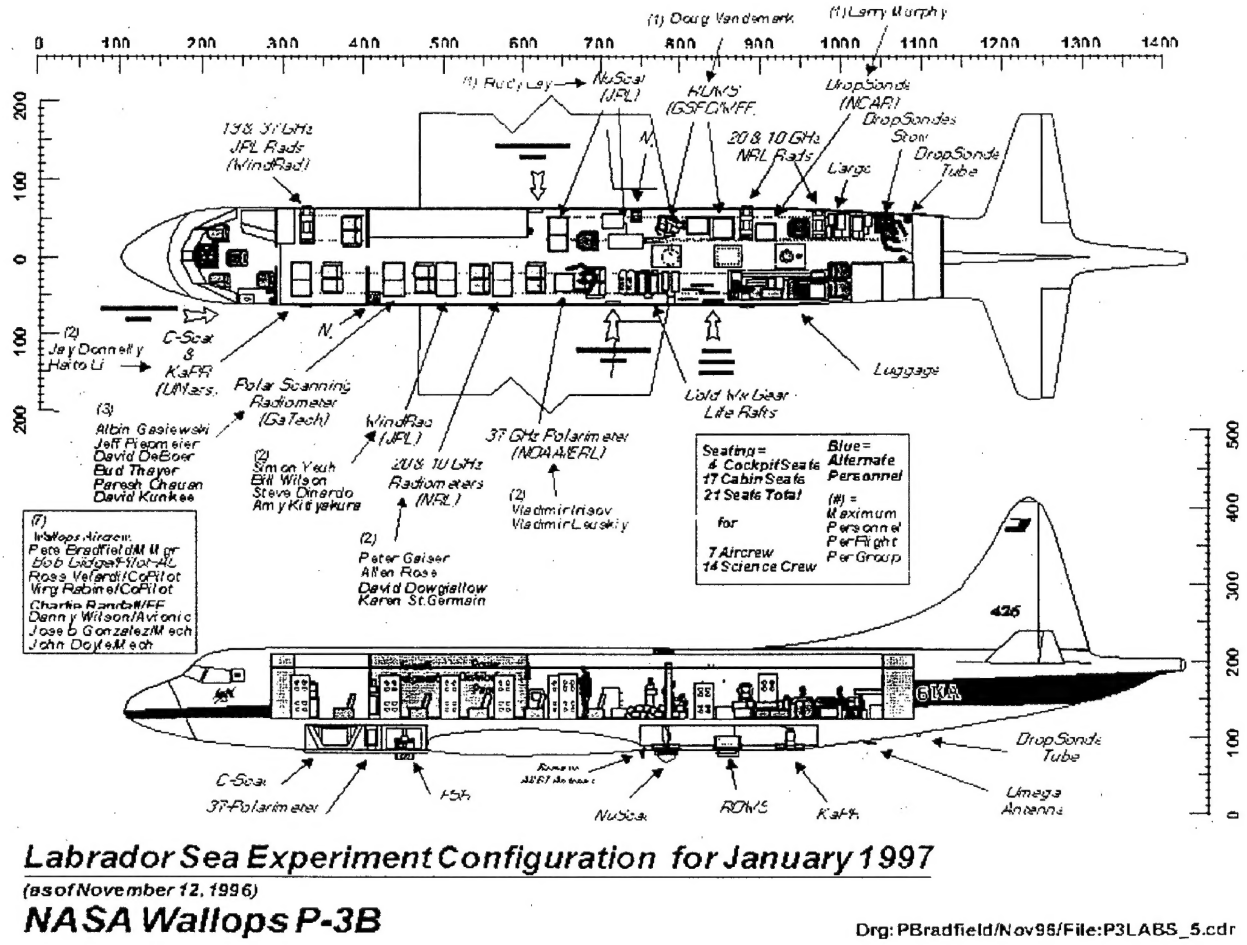

Figure 1: OWI Experiment: NASA Wallops P3 installation diagram.

CSCAT is a C-band pencil beam scatterometer. It measures the ocean backscatter simultaneously at 22.0°, 32.3°, 43.5° and 54.1° incidence, and by rotating its antenna in azimuth at 80 rpm, CSCAT measures the full azimuth backscatter response at four incidence angles every three-fourths of a second. KASPR is a Ka-band polarimetric radiometer that simultaneously measures the four brightness temperature Stokes parameters using a correlation receiver. For the OWI Experiment, a scan mirror was place in front of its horn antenna to squint the beam off at 47.5° incidence. The mirror was also rotated at 30 rpm about the center axis of the horn antenna in order to conically scan the beam. PSR contains four radiometers operating at 10.7, 18.7, 37 and 89 GHz. They are mounted on a Gimbel for conical and across track scanning, and each receiver measures the first three Stokes parameters. During the experiment, PSR mainly performed conical scans at 53° incidence. KAPOL is a Ka-band polarimetric radiometer that measures the brightness temperature Stokes vector. It was placed in a nadir viewing position for the experiment. ROWS is a Ku-band scatterometer, which acquires backscatter measurements with a nadir view antenna and a rotating antenna pointed at 16° incidence, from which the directional wave spectra can be derived.

The OWI experiment consisted of five flights (3, 4, 7, 9 and 10 March, 1997). Each mission was centered over the research vessel Knorr, which located at approximately 57°N, 53°W. During the flights, several hex cross patterns were executed over the ship. Figure 2 shows an illustration of the hex pattern, and one of the flight tracks from 4 March, 1997, is plotted. Wind vector estimates, derived from the CSCAT backscatter data using an algorithm based on the CMOD4 model function, are overlaid. For this flight the winds were fairly constant around 16 $m \cdot s^{-1}$ (32 knots) and the wind was from the West. The hex cross patterns provided 30-50 km flight lines crossing over the Knorr at three different approach angles. By approaching at several different angles, KAPOL observes the surface at different angles with respect to the wind direction, and any errors due to platform geometry and installations can be determined.

Surface winds from approximately 8 to 16 $m \cdot s^{-1}$ were sampled during the experiment. Using the CSCAT backscatter data, wind speed and direction estimates have been derived and colocated with KASPR data. Figure 3 plots a histogram of the colocated wind speed estimates. The majority of winds were between 10 and 14 $m \cdot s^{-1}$. Figure 4 plots a histogram of the difference between the wind direction estimates and the heading of the aircraft. This angle, which will be referred to as χ, varied from 0 to 360°. That is, several different headings where flown relative to the surface wind direction.

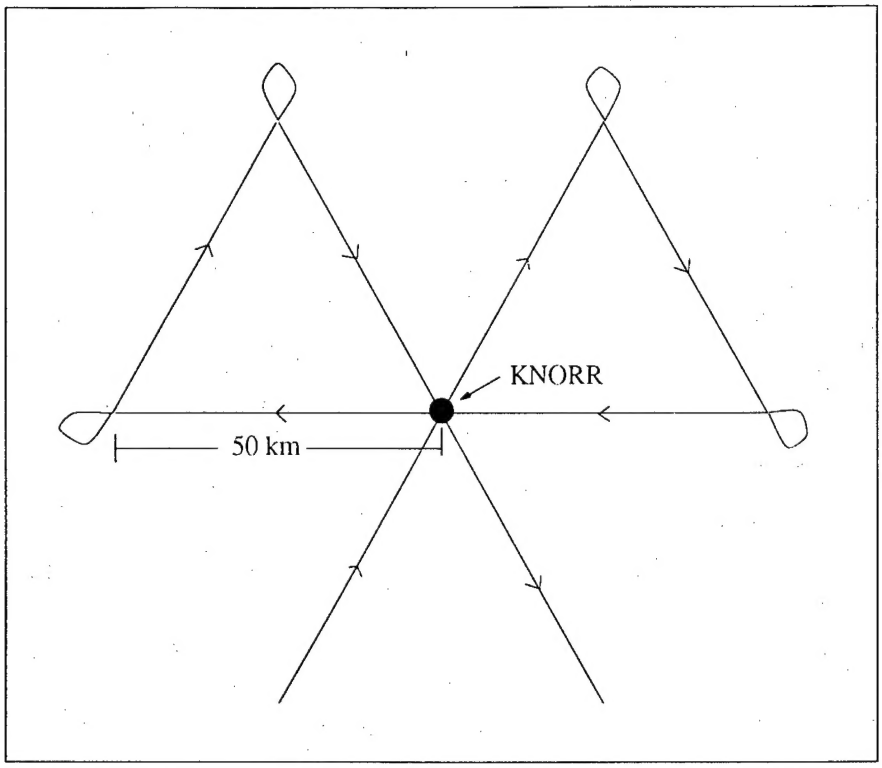

(a.)

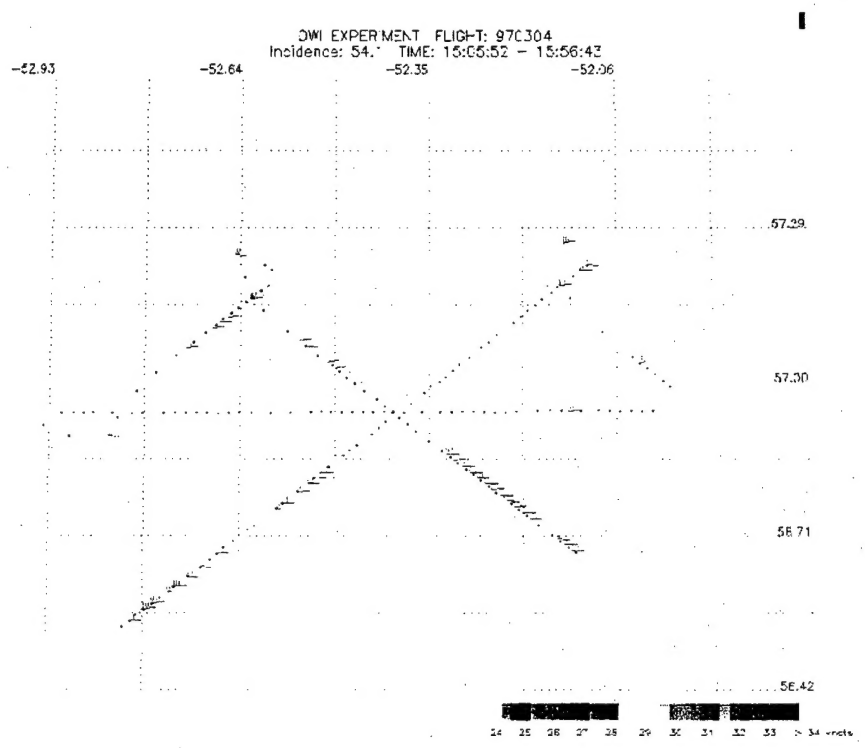

(b.)

Figure 2: (a) Hex cross pattern is illustrated. (b) Surface wind vector estimates are shown for a hex cross pattern executed on 4 March. 1997.

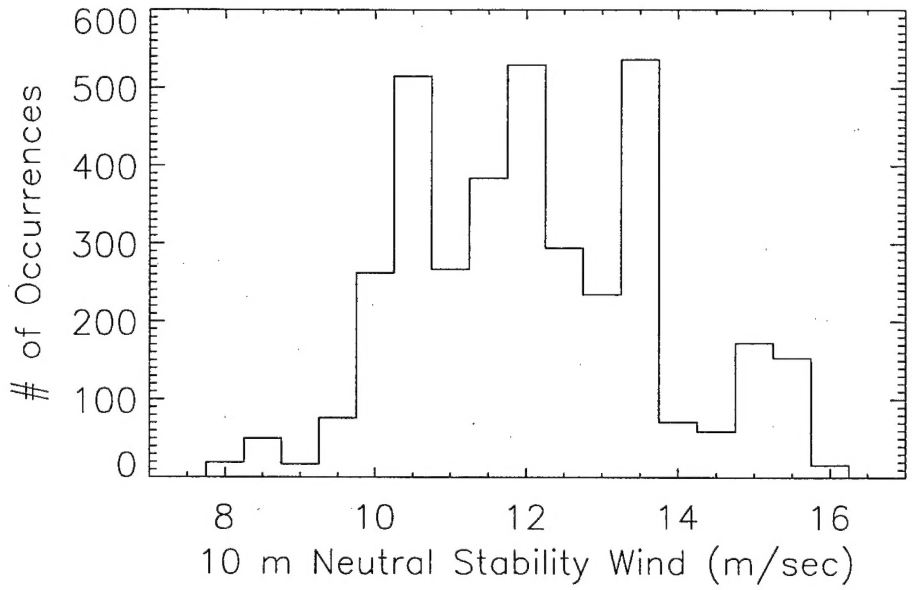

Figure 3: A histogram of the surface wind speeds sampled during the OWI Experiments is shown. The wind speeds estimates are derived from CSCAT data that were coincident with KASPR data.

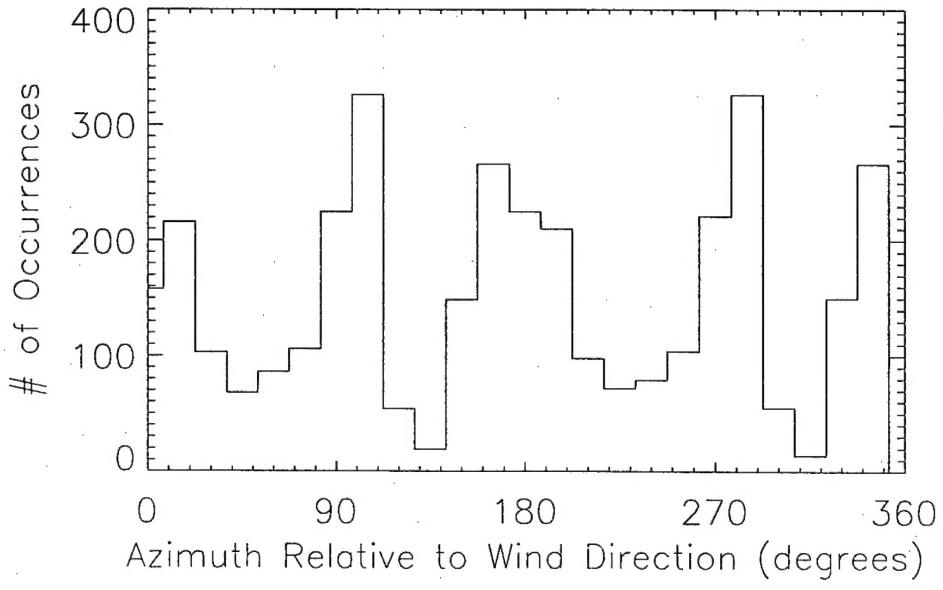

Figure 4: A histogram of the angle between the heading of the aircraft and the estimated surface wind direction is plotted. The wind direction estimates are derived from CSCAT data.

Data Summary

CSCAT and KASPR collected over thirty hours of measurements during OWI Experiment. Figure 5 plots the four brightness temperature Stokes parameters measured by KASPR for one conical scan. The wind speed and direction were approximately 15 $m \cdot s^{-1}$ and 270°. A few things are immediately obvious from this plot. The first two channels are displaying more than 50 K modulation with azimuth and are opposite one another. This is caused by the scan mirror which rotates the antenna polarization axis relative to the surface. At 0° and 180° rotation angle, channel 1 is measuring the horizontally polarized brightness temperature (T_h) and channel 2 is measuring the vertically polarized brightness temperature (T_v). The opposite is true for rotation angles 90° and 270°. At odd multiples of 45°, the two channels are measuring both T_v and T_h equally. The relationship between the brightness temperature measured by the four channels and the ocean surface brightness temperature Stokes vector is

$$\begin{bmatrix} T_v(\theta,\phi) \\ T_h(\theta,\phi) \\ U_B(\theta,\phi) \\ V_B(\theta,\phi) \end{bmatrix} = M \begin{bmatrix} T_2(\theta,\phi,\alpha) \\ T_1(\theta,\phi,\alpha) \\ T_3(\theta,\phi,\alpha) \\ T_4(\theta,\phi) \end{bmatrix} \tag{1}$$

where

$$M = \begin{bmatrix} cos(\alpha)^2 & sin(\alpha)^2 & \frac{1}{2} \cdot sin(2 \cdot \alpha) & 0 \\ sin(\alpha)^2 & cos(\alpha)^2 & -\frac{1}{2} \cdot sin(2 \cdot \alpha) & 0 \\ sin(2 \cdot \alpha) & -sin(2 \cdot \alpha) & -cos(2 \cdot \alpha) & 0 \\ 0 & 0 & 0 & -1 \end{bmatrix},$$

and α is the rotation angle of the mirror relative to the vertical polarization axis of the antenna, T_v is the vertical brightness temperature, T_h is the horizontal brightness temperature, U and V are the real and imaginary parts of the cross correlation of T_v and T_h, and T_1, T_2, T_3 and T_4 are the brightness temperatures outputs of channels 1, 2, 3 and 4 of KASPR. Note that channel 3 and 4 are the real and imaginary parts of the cross correlation of channels 1 and 2. Since all four Stokes parameters are measured, any polarization state can be realized.

The above equation also explains why the third channel exhibits more than 100 K modulation. The difference between T_v and T_h can exceed 50 K and therefore dominate the third channel at rotation angles that are centered around odd multiples of 45°. Another interesting feature to note is that the fourth channel is independent of the rotation angle and is only proportional to V. This is an ideal case which ignores cross-pol and direct leakage, but nevertheless the fourth channel only exhibits a very small modulation. This modulation might be caused by surface effects (referred. related to wind direction) or may be leakage signals.

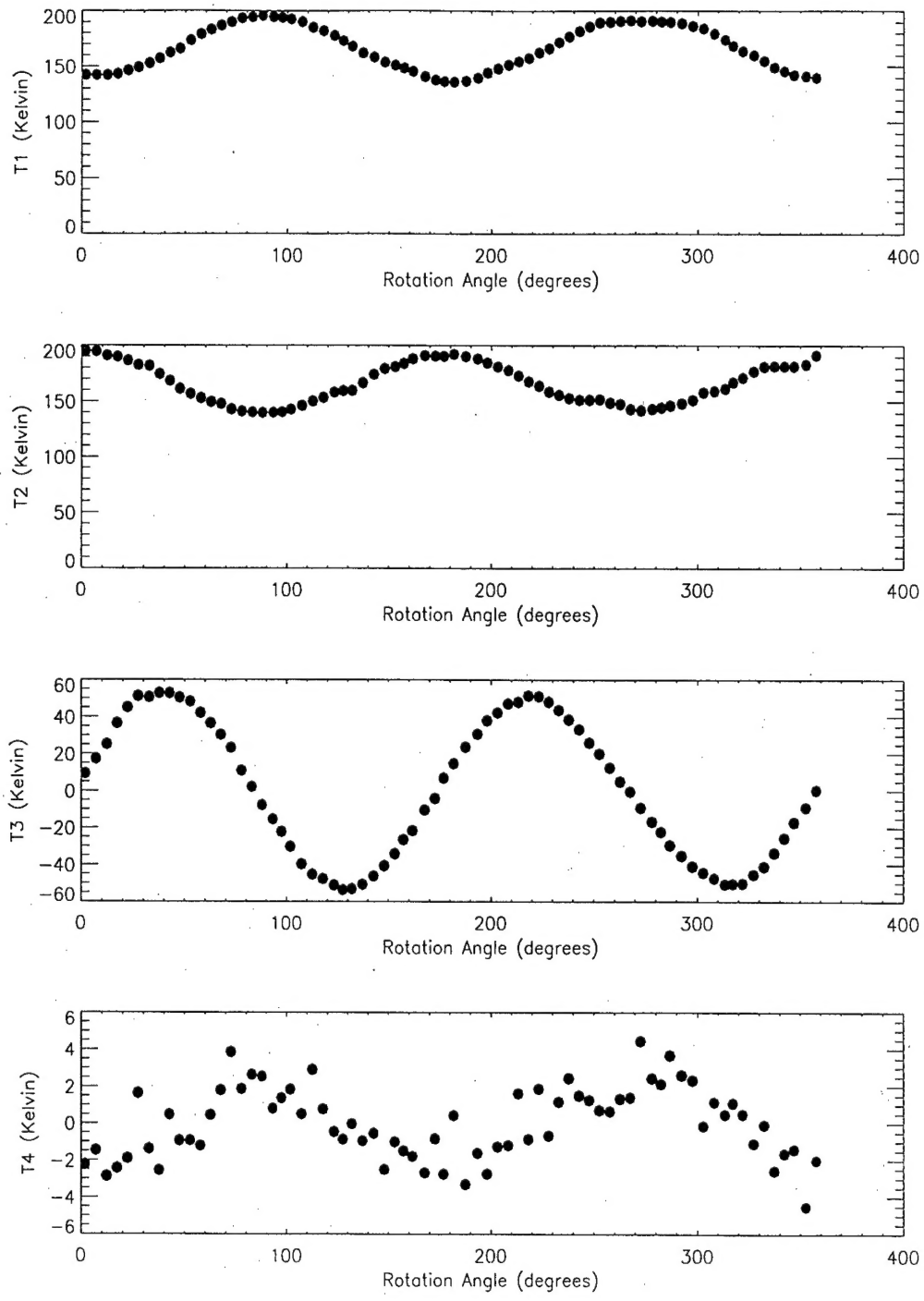

Figure 5: A single scan of brightness temperature measurements made with KASPR is plotted versus the rotation angle of the scan mirror.

To determine which is true, the other three channels need to be unscrambled using the relationship given by (1). However, this requires accurate calibrations of the first three channels to translate the voltage outputs to brightness temperatures. To calibrate the first two channels, a liquid nitrogen and an ambient load were used as reference loads and the slopes and offsets of the null feedback control circuits were determined. To calibrate the third and fourth channel, a polarized calibration load was constructed with a liquid nitrogen load, an ambient load and a wire grid. This polarimetric load was rotated in front of the antenna and the phase shift between the third and fourth channel was set to 45° so that both channels are proportional to U. From this, the gains of the two channels were calculated.

Results

The KASPR measurements obtained at rotation angles 0°, 90°, 180° and 270° were colocated with CSCAT wind speed and direction estimates. These angles were chosen so that the measured brightness temperature Stokes vector corresponded to the surface brightness temperature Stokes vector (i.e. no polarization mixing). Figure 6 plots T_v and T_h measurements versus colocated U_{10N} estimates. Red circles are points derived from channel 1 data and blue circles are points derived from channel 2 data. There seems to be no bias between the two channels which indicates that the calibration of these channels is correct. Furthermore T_v shows very little to no dependence on wind speed, while T_h is quite sensitive.

The vertical and horizontal brightness temperatures, shown in figure 6, are accumulated into .5 $\mathrm{m{\cdot}s^{-1}}$ bins and averaged. Figure 7 plots the averaged values versus wind speed (solid circles). The vertical lines mark the standard deviation of the measurements within each bin. At 47.5° incidence, the vertical brightness temperature should be insensitive to wind speed, while the horizontal brightness temperature should increase approximately 1 K for a 1 $\mathrm{m{\cdot}s^{-1}}$ increase in the wind speed. The following equations are fitted to the data using linear regressions,

$$T_v = C_0 + C_1 \cdot U_{10N} \tag{2}$$

and

$$T_h = D_0 + D_1 \cdot U_{10N}, \tag{3}$$

where U_{10N} is the 10 m neutral stability wind speed, and are over plotted as solid lines. The slopes (C_1 and D_1) are 0.1 and 0.7 $\mathrm{K/m{\cdot}s^{-1}}$ for vertical and horizontal polarized brightness temperature measurements, respectively. Corrections due to atmosphere attenuation and contribution have not been applied which slightly reduces the sensitivity of the measurements to the surface emission.

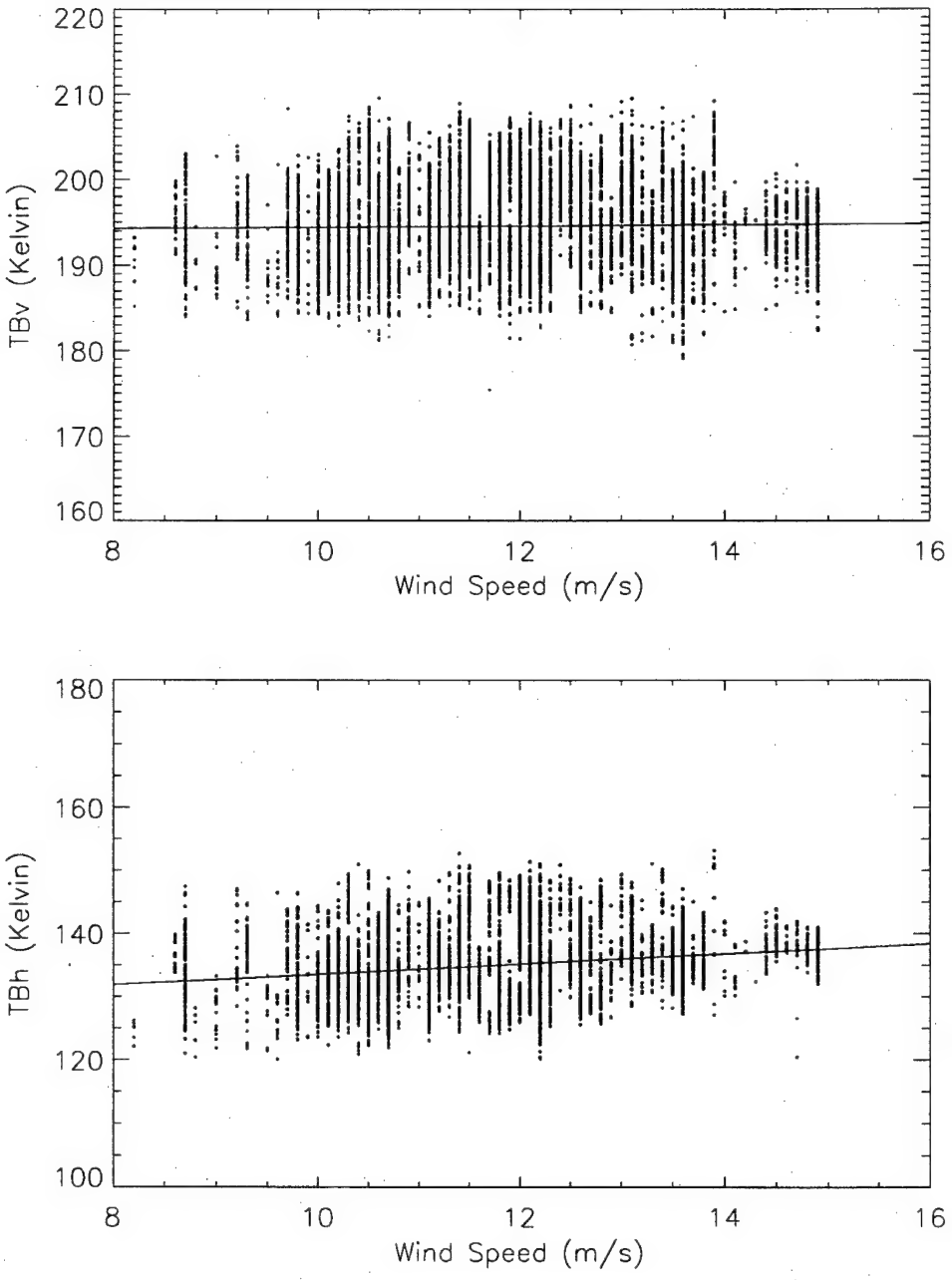

Figure 6: Vertical and horizontal brightness temperature measurements are plotted versus colocated wind speed measurements derived from CSCAT data. Brightness temperature measurements derived from channel one are color coded red and channel two are colored coded blue.

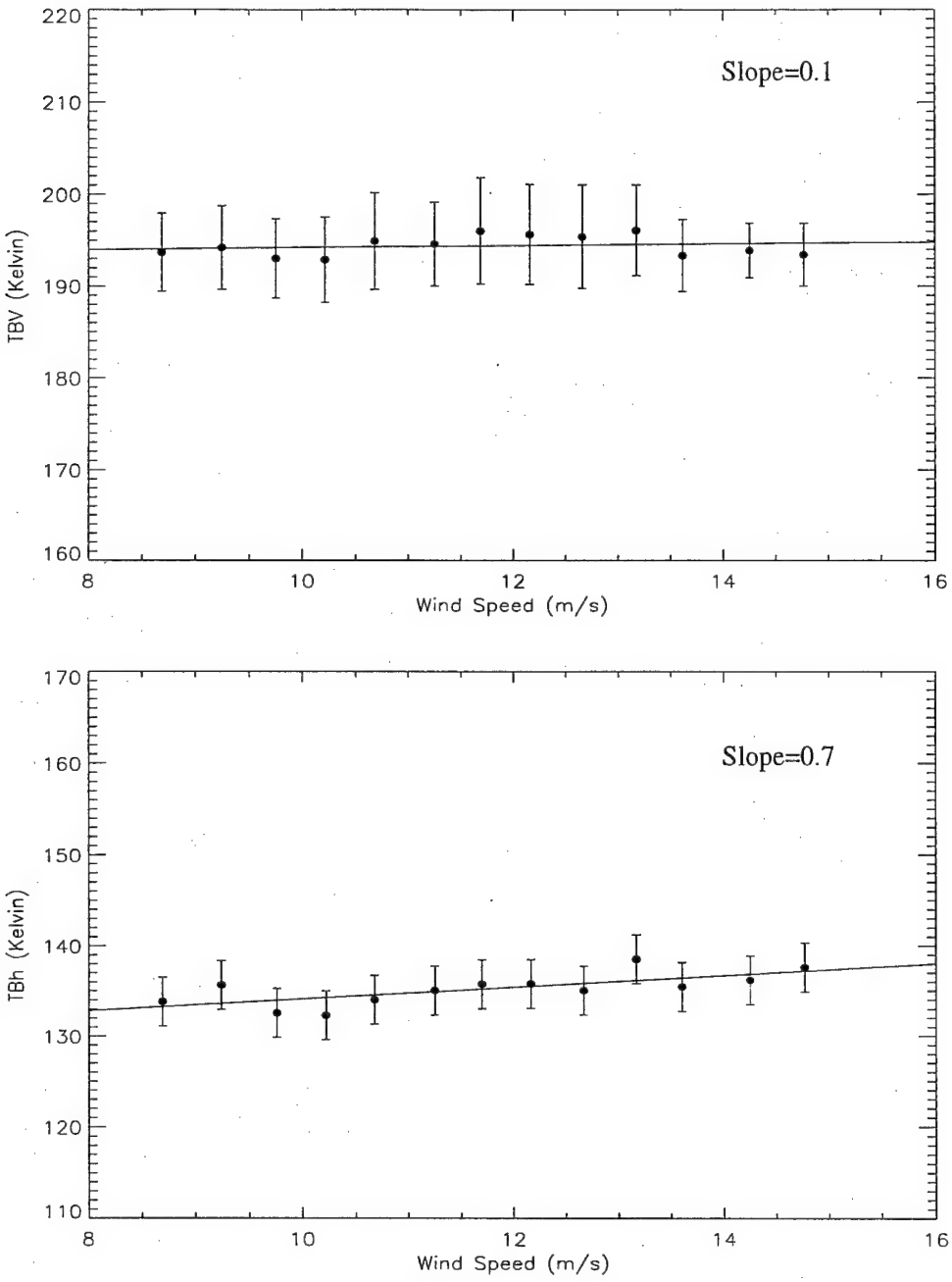

Figure 7: Averaged vertical and horizontal brightness temperature measurements are plotted versus colocated wind speed estimates. The data have been averaged into .5 $m \cdot s^{-1}$ wind speed bins. The standard deviations of the measurements within each bin are shown by the vertical lines. The solid lines represent a linear regressions between the vertical and horizontal brightness temperature measurements and the wind speed estimates.

The dependence of the T_v and T_h measurements on the instantaneous incidence angle (θ_i) was also evaluated. The measurements were limited to cases where the pitch and roll variations were less than 1 degree to eliminate any significant effects caused by the antenna polarization axis rotating relative to the surface due to the platform attitude. With this constraint, the instantaneous incidence angle varied only +/- 1°. Over this small range the dependence of T_v and T_h on incidence angle can be estimated as linear. Figure 8 plots the vertical and horizontal brightness temperature measurements as a function of the instantaneous incidence angle. The data has been averaged into 0.1° incidence angle bins. The following equations are fitted to the data using linear regressions,

$$T_v = C_2 + C_3 \cdot \theta_i \tag{4}$$

and

$$T_h = D_2 + D_3 \cdot \theta_i, \tag{5}$$

and are over plotted as solid lines. The sensitivity of the vertical and horizontal polarized brightness temperatures are approximately 2 K/degree and -1.3 K/degree, respectively, which is consistent with theory. Note that the standard deviation of the T_h measurements is larger than the T_v measurements. This occurs because T_h is much more sensitive to changes in the wind speed.

The final goal is to determine the dependence of the four brightness temperature Stokes parameters on wind direction. To do so, we must first unscramble the polarization mixing on a scan by scan basis. The calibration of channels 3 and 4 is still being refined so equation (1) can yet be applied. However, using the data obtained at rotation angles 0°, 90°, 180° and 270°, a qualitative analysis can be performed to evaluate the functional dependence of T_v and T_h on wind direction. This is accomplished by calculating the difference between the KASPR look direction (aircraft heading plus rotation angle) and the wind direction is calculated for each colocated point. This angle (χ) represents KASPR's look direction relative to the wind direction. The T_v and T_h measurements are then accumulated into 15° azimuth bins according to χ and averaged. Figure 9 plots these values versus χ. The two Fourier series shown below are fitted to the data,

$$A_0 + A_1 \cdot cos(\chi) + A_2 \cdot cos(2 \cdot \chi) \tag{6}$$

and

$$A_0 + A_1 \cdot cos(\chi) + A_2 \cdot cos(2 \cdot \chi) + B_1 \cdot sin(\chi) + B_2 \cdot sin(2 \cdot \chi). \tag{7}$$

The cosine series is shown by the solid line and the cosine-sine series is shown by the dashed line. The sine terms (B_1 and B_2) are small compared to the cosine terms. Therefore, the

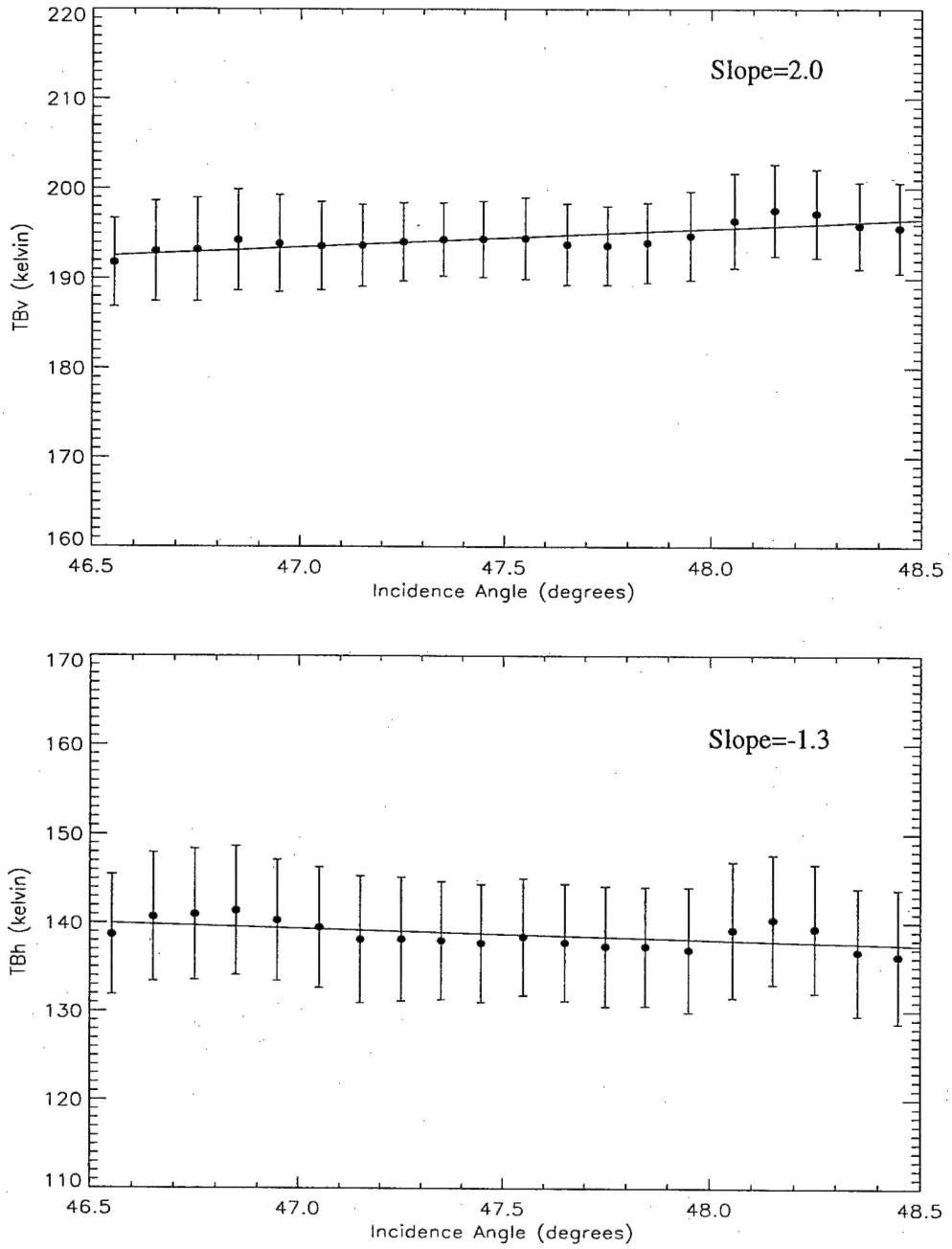

Figure 8: Averaged vertical and horizontal brightness temperature measurements are plotted versus instantaneous incidence angle. The data have been averaged into .1° incidence angle bins. The standard deviations of the measurements within each bin are shown by the vertical lines. The solid lines represent a linear regressions between the vertical and horizontal brightness temperature measurements and the instantaneous incidence angle.

wind direction signatures can be represented using only the Fourier cosine series. Furthermore for vertical polarization, A_2 is also small compared to A_1, thus the vertical brightness temperature can be described by using only the first two terms of the Fourier cosine series. The horizontal brightness temperature is best described using all three Fourier cosine terms. This is consistent with results published by Wentz (IEEE TGARS, 1992) for moderate wind cases.

Conclusions

The data set collected during the OWI experiment will significantly aide in determining the potential of polarimetric radiometry for remote sensing of the ocean wind vector. Current collaboration amongst the groups participating in this experiment has led to a conference paper on the subject that was present at IGARSS '97 and a manuscript expanding on the conference paper will be submitted this spring to IEEE Transactions on Geoscience and Remote Sensing. The results presented in this report have shown a wind directional signature in T_v and T_h. Once the individual scans have been unscrambled, a full Fourier analysis will be performed to determine which components are statistically significant in describing the modulation of each brightness temperature Stokes parameters. Given the range of sampled wind speed, the dependence of the Fourier components on wind speed may also be determined.

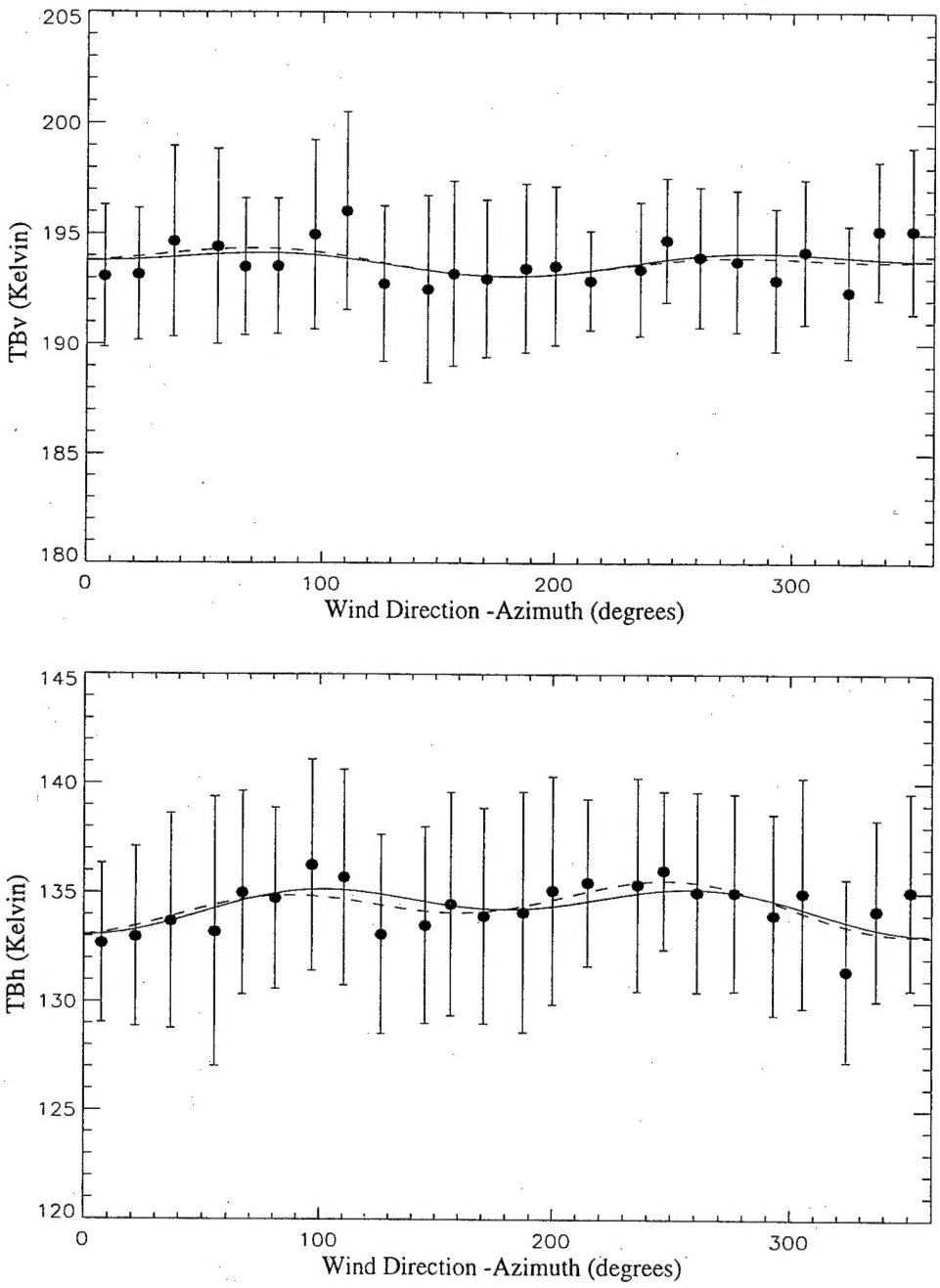

Figure 9: Averaged vertical and horizontal brightness temperature measurements are plotted versus colocated azimuth look direction relative to surface wind direction. The data have been averaged into 15° azimuth bins. The standard deviations of the measurements within each bin are shown by the vertical lines. The solid and dashed lines are the regression fit of (6) and (7) to the data.